

Contaminant Flow and Transport Simulation in Cracked Porous Media Using Locally Conservative Schemes

Pu Song¹ and Shuyu Sun^{1,2,*}

¹ Department of Mathematical Sciences Clemson University, Clemson, SC 29634, USA

² Computational Transport Phenomena Laboratory (CTPL), Division of Physical Sciences and Engineering (PSE), King Abdullah University of Science and Technology (KAUST), 4700 King Abdullah University of Science and Technology, Thuwal 23955-6900, Kingdom of Saudi Arabia

Received 5 January 2011; Accepted (in revised version) 11 December 2011

Available online 10 July 2012

Abstract. The purpose of this paper is to analyze some features of contaminant flow passing through cracked porous medium, such as the influence of fracture network on the advection and diffusion of contaminant species, the impact of adsorption on the overall transport of contaminant wastes. In order to precisely describe the whole process, we firstly build the mathematical model to simulate this problem numerically. Taking into consideration of the characteristics of contaminant flow, we employ two partial differential equations to formulate the whole problem. One is flow equation; the other is reactive transport equation. The first equation is used to describe the total flow of contaminant wastes, which is based on Darcy law. The second one will characterize the adsorption, diffusion and convection behavior of contaminant species, which describes most features of contaminant flow we are interested in. After the construction of numerical model, we apply locally conservative and compatible algorithms to solve this mathematical model. Specifically, we apply Mixed Finite Element (MFE) method to the flow equation and Discontinuous Galerkin (DG) method for the transport equation. MFE has a good convergence rate and numerical accuracy for Darcy velocity. DG is more flexible and can be used to deal with irregular meshes, as well as little numerical diffusion. With these two numerical means, we investigate the sensitivity analysis of different features of contaminant flow in our model, such as diffusion, permeability and fracture density. In particular, we study K_d values which represent the distribution of contaminant wastes between the solid and liquid phases. We also make comparisons of two different schemes and discuss the advantages of both methods.

AMS subject classifications: 65M12, 65M15, 65N30, 76D07, 76S05

Key words: Mixed finite element methods, discontinuous Galerkin methods, reactive transport equation, flow equation.

*Corresponding author.

URL: <http://web.kaust.edu.sa/faculty/ShuyuSun/>

Email: shuyu.sun@kaust.edu.sa (S. Y. Sun), pus6@pitt.edu (P. Song)

1 Introduction

In this paper, we are interested in simulating processes in subsurface waste repositories. We have a solid concrete matrix to seal the radioactive wastes underground, however, there will be some fractures produced by the erosion of water, acid solute or other undetermined elements during the long time periods. Hence, we need to consider how these radioactive wastes leak through our concrete matrix from these apertures since the convection in fractures is much faster than that in matrix. Although this scenario is complicated to model exactly, we make reasonable simplification to create a mathematical model that can be handled numerically and yet produce accurate prediction. We shall construct a mathematical model as follows: we will consider the flow of an incompressible fluid through a homogeneous saturated porous media, where the fluid is contaminated by a solute, with concentration $c \geq 0$. We assume that the flow is at steady state and that transport is described by advection, molecular diffusion, mechanical dispersion, and chemical reaction (adsorption) between solute and the surrounding solid porous skeleton. There are lots of applications related to this model [2,9,15,16,25,30,31,33].

The contaminant flow of fluids through fractures is a process that plays an important role for many areas of the geosciences. Research on fluid flow in fractures and in fractured porous media has a history that spans nearly four decades. This research can be classified as four principal aspects of fracture flow: 1) development of conceptual models, 2) development of analytical and numerical solution schemes, 3) description of fracture hydraulic characteristics in static and deforming media, and 4) development of stochastic techniques to describe fracture flow and hydro-geologic parameter distributions. In this paper, we will firstly build the mathematical model for the original problem, then apply appropriate numerical schemes to solve this model and analyze the numerical results from our proposed methods in order to derive a better solution and accurate results.

Several conceptual models have been developed for describing contaminant fluid flow in fracture porous media. Fundamentally, each method can be distinguished on the basis of storage and flow capacities of the porous medium and the fracture. The storage characteristics are associated with porosity, and the flow characteristics are associated with permeability. There are three conceptual models which dominated the research so far: 1) dual continuum, 2) discrete fracture network, 3) single equivalent continuum. In addition, multiple-interacting continua and multi-porosity/multi-permeability conceptual models (Sahimi [24], 1995) have recently been introduced into literature. Further distinctions can be drawn on the basis of spatial and temporal scales of integration, or averaging, of the flow regime. In our research, we will mainly focus on discrete fracture network [20,21], which preserves physics closely.

After we built the mathematics model, we need to solve it with numerical algorithms. For different parts of our models, we deal with them by specific methods in order to obtain best simulation results. The movement of contaminants through the fractured porous medium is modeled by transport equations; that is, equations which

describe the advection, diffusion and interaction of contaminants within the environment. These equations are often advection-dominated, and thus require special care when solved numerically. In recent years, there has been much interest in using upwind schemes for simulating such transport problems. These schemes can also be improved to high resolution or shock-capturing methods. In this paper, we employ an upwind-mixed finite element/finite volume method to deal with transport and flow equation due to the advantage of Finite Volume Method (FVM) in dealing with advection part of transport equation and Mixed Finite Element (MFE) method in dealing with flow and diffusion, adsorption part of transport equation. On structured grids, using special numerical integration rules, the upwind-mixed method is equivalent to a cell-centered finite difference method, which is much easier to handle and code. We also investigate the Discontinuous Galerkin (DG) method [26–29] for advection part of transport equation since DG method can be a locally conservative, stable, high-order accurate, flexible, less numerical diffusion and easy implemented method which can easily handle complex geometries, irregular mesh with hanging nodes and also can be easily coupled with other methods like conforming mixed finite element methods.

Substantial research has been published in various aspects of the contaminant flow in fractured porous medium. For example, Shinichi Nakayama and Ikuji Takagi et al. [23] (1986) studied the advection-diffusion migration of radionuclide through two-layer geological media. Clint Dawson [10] (1998) used upwind-mixed finite element method to solve nonlinear contaminant transport models. Vandym Aizinger and Dawson, et al. [1] (2001) used local DG to simulate contaminant flow models.

This paper is divided into following sections: First, the differential equations describing the contaminant diffusion and transport in the fractured cementitious matrix are presented. Second, a numerical model in saturated fractured media is described. We discuss in detail various components of our numerical approach, which include the MFE method and cell centered finite difference method for the flow equation, the combined FVM-MFE method and DG-MFE method for the transport equation and the numerical discretization in time. We then present numerical examples in fractured media with various fracture distributions. For each example, we provide and discuss simulated concentration profiles at different times, together with pressure and velocity fields, and we also present some examples between MFE scheme and DG scheme to see the difference between two schemes. Finally, we numerically carry out a sensitivity analysis of parameters to our model and investigate the relationship between intrinsic K_d value and effective K_d value, also the relationship between fracture density and effective K_d value, and impact of impulse concentration on our models, all of which will help us design barriers that are protective of the public environment.

2 Mathematical model

When the contaminants leak through the porous medium, there will be adsorption, convection and diffusion brought by the movement of those contaminants. Therefore,

we use reactive transport equation to describe those phenomena during the periods of contaminants passing through the medium. We also need to use flow equation to govern the fluid flow and predict the pressure field and Darcy velocity field. Based on experimental data and above analysis, we construct mathematical model for contaminant species passing through the porous media, which include two coupled differential equations: one is flow equation which is an elliptic equation of unknown scalar variable pressure, the other one is reactive transport equation which is a parabolic equation used for describing adsorption, diffusion and convection of contaminant flows.

Let Ω denote a bounded polygonal domain in R^d , ($d = 2, 3$). The classical equations governing the miscible displacement of contaminants in porous medium are as follows:

2.1 Flow equation

The flow equation is obtained from the conservation of total fluid volume and Darcy's law [13,32]

$$-\nabla \cdot (K\nabla p) \equiv \nabla \cdot \mathbf{u} = q, \quad x \in \Omega, \quad (2.1)$$

and here K is the conductivity defined by:

$$K = \frac{k}{\mu}, \quad (2.2)$$

where p (the pressure in the fluid mixture) and \mathbf{u} (the Darcy velocity of the mixture, i.e., the volume of fluid flowing cross a unit across-section per unit time) are unknowns. The permeability tensor k of the medium measures the conductivity of the medium to fluid flow; the viscosity μ of the fluid measures the resistance to flow of the fluid mixture; the imposed external total flow rate q is a sum of source (injection) and sinks (extraction).

Darcy velocity is defined as follows:

$$\mathbf{u} = -\frac{k}{\mu}\nabla p. \quad (2.3)$$

The boundary conditions for our domain Ω are:

$$\begin{aligned} p &= p_B, & x &\in \Gamma_D, \\ \mathbf{u} \cdot \mathbf{n} &= u_B, & x &\in \Gamma_N, \end{aligned}$$

where $\Omega = \Gamma_D \cup \Gamma_N$, Γ_D denotes the Dirichlet boundary and Γ_N denotes the Neumann boundary.

2.2 Reactive transport equations

The reactive equation system is obtained from the mass conservation of considered contaminant species. It governs the convection, diffusion, and adsorption of contaminants and gives the concentration profile provided the velocity field is given from flow equation. The contaminant concentrations in the fluid and in the solid as well as their relation can be described by:

$$\begin{cases} \frac{\partial \Phi c}{\partial t} + \nabla \cdot (\mathbf{u}c - \mathbf{D}(\mathbf{u})\nabla c) = r(c, c_s), \\ \frac{\partial \rho c_s}{\partial t} = -r(c, c_s), \quad (x, t) \in \Omega \times (0, T], \\ c_s = K_d c. \end{cases} \quad (2.4)$$

Summation of the two concentration equations above (one in fluid and one in solid) yields:

$$\frac{\partial \Phi^{eff} c}{\partial t} + \nabla \cdot (\mathbf{u}c - \mathbf{D}(\mathbf{u})\nabla c) = 0, \quad (2.5)$$

where

$$\Phi^{eff} = \Phi + \rho K_d,$$

is the effective porosity and it is calculated separately for the matrix and for the fractures: in the matrix:

$$\Phi = \Phi_{matrix};$$

in the fracture: $\Phi = 1, K_d = 0, \Phi^{eff} = \Phi = 1.0$. The reason for this setting of porosity is due to the definition of porosity. The unknown variable c is the concentration of the interested species within the fluid (i.e., the amount of the species per unit volume of the fluid mixture) and c_s is the concentration of the interested species in the solid. T is the final simulation time. The parameter K_d is the partitioning coefficient of the considered species between the fluid and the solid. We will talk about the details of K_d in later section. ρ is the density of fluid mixture; the porosity Φ is the fraction of the volume of the medium occupied by pores and is assumed to be time-independent, uniformly bounded above and below by positive numbers; the dispersion-diffusion tensor $\mathbf{D}(\mathbf{u})$ has contributions from molecular diffusion and mechanical dispersion, and can be calculated by:

$$\mathbf{D}(\mathbf{u}) = d_m \mathbf{I} + |\mathbf{u}| \{ \alpha_l \mathbf{E}(\mathbf{u}) + \alpha_t (\mathbf{I} - \mathbf{E}(\mathbf{u})) \}, \quad (2.6)$$

where $d_m = \Phi \tau D_m$ and is assumed to be strictly positive; τ is the tortuosity coefficient; D_m is the molecular diffusivity; α_l and α_t are the longitudinal and the transverse dispersivities, respectively; $\mathbf{E}(\mathbf{u})$ is the tensor that projects onto the \mathbf{u} direction, whose (i, j) component is

$$\mathbf{E}(\mathbf{u}) = \frac{\mathbf{u}_i \mathbf{u}_j}{|\mathbf{u}|^2}.$$

We assume our domain Ω has Lipschitz boundary $\partial\Omega = \Gamma_{in} \cup \Gamma_{out}$, where Γ_{in} is the inflow boundary and Γ_{out} is the out flow boundary, which is defined as follows:

$$\begin{cases} \Gamma_{in} = \{c \in \partial\Omega : \mathbf{u}(x) \cdot \mathbf{n}_{\partial\Omega} < 0\}, \\ \Gamma_{out} = \{c \in \partial\Omega : \mathbf{u}(x) \cdot \mathbf{n}_{\partial\Omega} \geq 0\}, \end{cases}$$

where $\mathbf{n}_{\partial\Omega}$ is the unit outward normal vector to $\partial\Omega$. The boundary conditions for transport equation are defined as follows:

$$\begin{cases} (\mathbf{u}c - \mathbf{D}(\mathbf{u})\nabla c) \cdot \mathbf{n} = c_B \mathbf{u} \cdot \mathbf{n}, & x \in \Gamma_{in}, \quad t \in (0, T], \\ (-\mathbf{D}(\mathbf{u})\nabla c) \cdot \mathbf{n} = 0, & x \in \Gamma_{out}, \quad t \in (0, T]. \end{cases}$$

We specify an initial concentration in the following way:

$$c(x, 0) = c_0(x).$$

3 Numerical algorithms

In this paper, the system contains two parts: a flow equation involving the pressure (scalar variable) and Darcy velocity (vector variable), and a reactive transport equation for describing the evolution of contaminant concentrations. We first solve the flow equation by a MFE method; then we solve the reactive transport equation semi-implicitly (explicitly for convection and implicitly for diffusion and adsorption) in time by using a combination of FVM and MFE method and also employing a combination of DG and MFE method to treat advection and diffusion parts respectively.

3.1 Mixed finite element method

Mixed finite element method was initially introduced by engineers in the 1960's for solving problems in solid continua, which is a generalized finite element method [3,4,7,17]. The advantage for using the mixed method is that it can be used to approximate both vector variable (flux velocity) and scalar variable (pressure) simultaneously and to give a high order approximation of both variables. Compared with traditional finite element method, mixed method employed two different spaces to deal with two variables mentioned above, and these two spaces must satisfy inf-sup condition for the mixed method to be stable, which avoids to work with conventional finite element space, something which is difficult to use piecewise constant functions. Detailed formulation for mixed finite element method applied to the flow problem is listed in the appendix.

3.2 Discontinuous Galerkin method

Traditional Continuous Galerkin (CG) finite element method has been around for more than 60 years [5,6,14]. It is widely used for solving practical problems due to its

simple implementation comparing with MFE and DG method. However, with more requirements on the accuracy of solutions and high efficient computation, CG method cannot meet the needs of every problem. Thus, the investigation of MFE method and DG method draws lots of attention in recent years.

The DG method has many attractive features compared with the CG method. For example, the cross-element communication is more expensive in CG than it in DG, which makes DG more attractive for parallel computation. The DG method is locally mass conservative at the element level while CG method only satisfies a global mass balance over the whole computational domain. The property of mass conservation is crucial in flow and transport problems, especially in convection-dominated problems. In addition, it has less numerical diffusion and provides more local approximation than most conventional algorithms. The success of this method is mainly due to three facts. First, the nonlinear conservation laws are enforced locally; second, when the approximate solution is not piecewise constant, the stability of the method does not follow from the form the numerical fluxes anymore and has to be enforced by means of flux or slope limiter; third, both the approximate solution and associated fluxes can experience discontinuities across inter-element boundaries due to its discontinuous function space. But for CG methods or other traditional algorithms, they must enforce continuity condition when crossing the inter-element boundaries. Because of local property of DG method, the trial and test spaces are easier to construct than conforming methods, which renders the code shorter and more efficient for DG method. Unlike mixed finite element methods or traditional continuous Galerkin methods which not only care about information of interface and elements but also include vertices of each element, DG method just needs to handle the information of elements and interfaces, which make the code more reliable.

There are only two popular families of DG methods. One is primal DG method, namely variations of interior penalty methods which include symmetric interior penalty Galerkin (SIPG), incomplete interior penalty Galerkin (IIPG,) and non-symmetric interior penalty Galerkin (NIPG) methods; the other is mixed DG methods which have been systematically investigated by B. Cockburn and C. W. Shu and others. Both methods have their attractive features, but we will use the primal DG in this paper. Detailed formulation for mixed finite element method applied to the transport problem is listed in the Appendix.

3.3 Stability analysis

We used mixed finite element method based on RT_0 space for the flow equation, which has been proved to be stable in the literature [8, 22]. After we got the Darcy velocity from flow equation, we plugged it into transport equation; then applied backward Euler method to get the final solution, which has been proved to be stable in many literatures. Also for each numerical example, the plots of the flow weighted mean concentration versus time indicated that our algorithm is stable for the coupled system [11].

4 Numerical results on rectangular meshes

4.1 Simulation examples (MFE scheme)

According to experimental data, we construct a computational domain of $(0, 0.6m) \times (0, 0.6m)$ for all numerical examples. We used a uniform time step to run the simulations, each time steps take 100 years. We also use non-uniform rectangular mesh to discretize a $(0, 0.6m) \times (0, 0.6m)$ rectangular domain with random fractures for our simulation.

Among our simulation examples, Example 4.1 is the base case to be compared with other examples. In this base case, we use a set of standard parameters from laboratory (see Table 1). In other examples we vary the fractures with different lengths and distributions, but maintain the same parameters with base case. In all examples, we assume no-flow boundary conditions on both top ($y = 0m$) and bottom boundaries ($y = 0.6m$). We also specify a constant pressure of 0 (gauge pressure against a reference pressure) on the right boundary ($x = 0.6m$). Contaminant species is injected on the inflow boundary located on the left ($x = 0m$), where a higher pressure condition of 1 $m-H_2O$ is imposed. The medium is initially saturated with clean water.

Example 4.1. Three horizontal and two vertical fractures (Base Case)

Table 1: Standard parameters.

Saturated Hydraulic Conductivity K_s (cm/s)	Saturated Effective Diffusion Coefficient D_e (cm ² /s)	Effective Porosity (%)	K_d value (ml/g)
1.0E-12	5.0E-11	18.4	0

We use parameters listed in Table 1 for our base case and the total simulation time is 10,000 years. The fracture network involves three horizontal and two vertical fractures that are interconnected (Fig. 1). We generate non-uniform rectangular mesh for this fractured media due to efficiency. As described before, we apply MFE for the flow equation, and semi-implicit FVM-MFE for the transport equation using a uniform time step of 100 years. The simulated pressure field (Fig. 2) clearly indicates the influence of the fractures on the flow. We could see that there is a sharp peak when the inlet and outlet of fracture network does not touch the matrix boundary. If the inlet of fracture network extends to the boundary of our domain, then contaminant species pass through the fracture immediately, the pressure field will not be too much different from that in the matrix. Velocity fields are displayed in the streamline/quiver plot (Fig. 2). As expected, the magnitude of the velocity is much smaller in the matrix as compared to it in the fracture. Moreover, it can be observed that streamlines tend to converge into fractures in the left part of the domain but diverge from the fractures in the right part, which suggests that fractures are the main pathways for transporting contaminants via convection. Fig. 3 gives results of simulated concentration profiles at different times (only 300 years and 5,000 years shown). At 100 years to 1000 years, the contaminant transports mainly through the convection within fractures. This is clearly demonstrated by the concentration plume formed quickly at the fracture outlets while

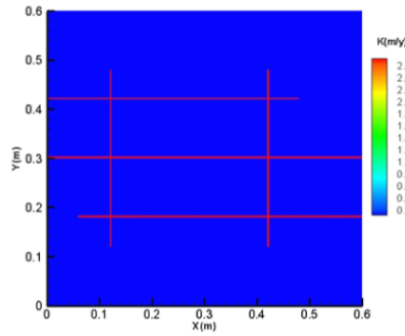


Figure 1: Fracture and conductivity distribution for base case.

the matrix closer to the inflow boundary is still quite clean. After 2,000 years, diffusion and convection via the matrix also start to play a significant role in the overall contaminant transport behavior.

The flow weighted mean concentration in effluent fluid as a function of time is provided in Fig. 4. We note that the flow weighted mean concentration quickly increases to 0.999, and then slowly approaches to 1. This is because the fracture network here connects inflow and outflow boundaries, which creates a flow shortcut and leads to

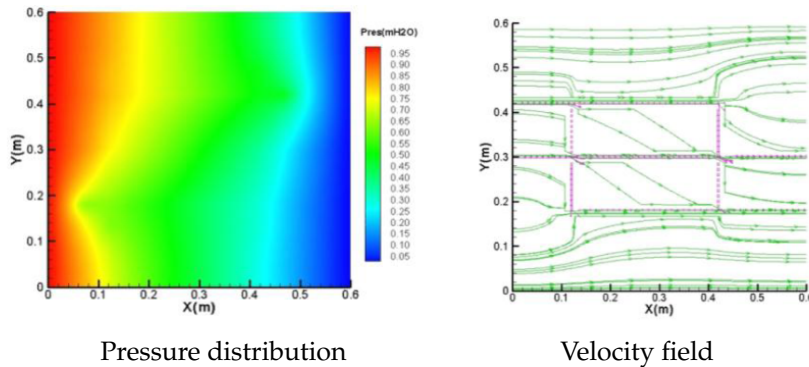
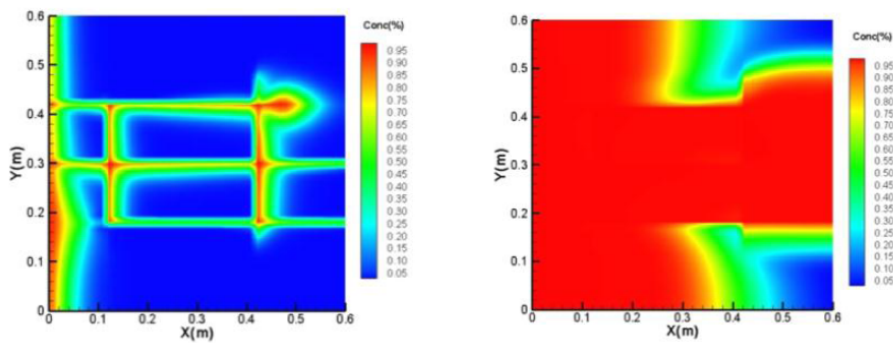


Figure 2: Pressure distribution and Velocity field for Example 4.1.



Concentration distribution at 300 year Concentration distribution at 5000 year
 Figure 3: Concentration at different time within ten thousand years.

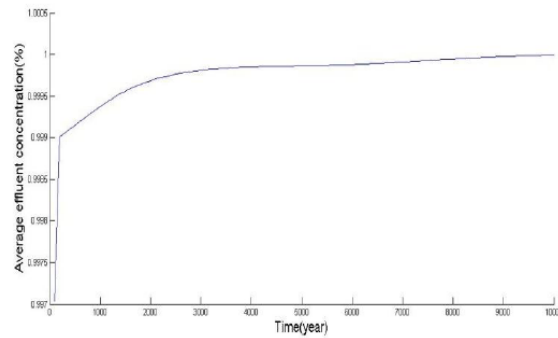


Figure 4: The flow weighted mean concentration versus time for Example 4.1.

almost all fluid exiting from the cracks rather than from the matrix.

Example 4.2. Five horizontal and three vertical fractures (within medium interior)

Similar to Example 4.1, we employ the model parameters listed in Table 1 and we also simulate up to 10,000 years. We impose Neumann boundary condition (10^{-4} m/year) on the left boundary and Dirichlet boundary condition (0 m- H_2O) on the right boundary. Unlike previous crack setting, the fracture network in this case involves five horizontal and three vertical fractures that are interconnected, but do not extend to the boundary (Fig. 5). We apply RT_0 -MFE on rectangular meshes for the flow equation, and semi-implicit FVM-MFE for the transport equation using a uniform time step of 100 years. The simulated pressure field (Fig. 6) clearly indicates the influence of the fractures on the flow. The velocity fields are displayed in the streamline/quiver plot (the right panel of Fig. 6). Again, the magnitude of the velocity is much smaller in the matrix as compared to it in the fracture. Moreover, it can be observed that streamlines tend to converge into fractures near the inflow boundary but diverge from the fractures close to the outflow boundary. Obviously, we observe one more time that fractures are the main pathways for transporting contaminants via convection. Fig. 7 are results of simulated concentration profiles at different times (300 years and 5000 years) from rectangular mesh simulation. At early simulation times, the contaminant transports mainly through the convection within fractures. This is clearly demonstrated by the fact that the concentration plume is formed quickly at the fracture outlets while the matrix closer to the inflow boundary is still quite clean. At later simulation times, diffusion and convection via the matrix also start to play a significant role in the overall contaminant transport behavior. Fig. 8 depicts the relationship between flow weighted mean concentration and time. We note that the flow weighted mean concentration does not quickly increase to 0.999 within a short time, cause our fracture network does not extend to the inflow and outflow boundaries, thus it leads our curve smoothly increasing before the contaminant species reaches the fracture network and also increasing smoothly when it comes out from fracture network, therefore we can see a breakthrough curve (a smooth step function) in this example. In about ten thousand years, the average normalized concentration on outflow boundary reaches about 99%.

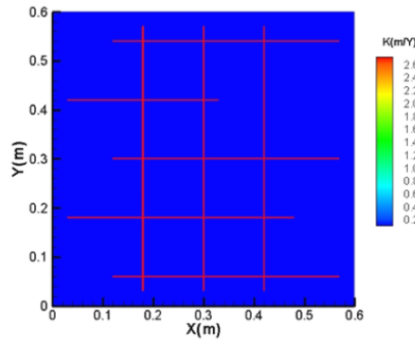


Figure 5: Fracture and conductivity distribution for Example 4.2.

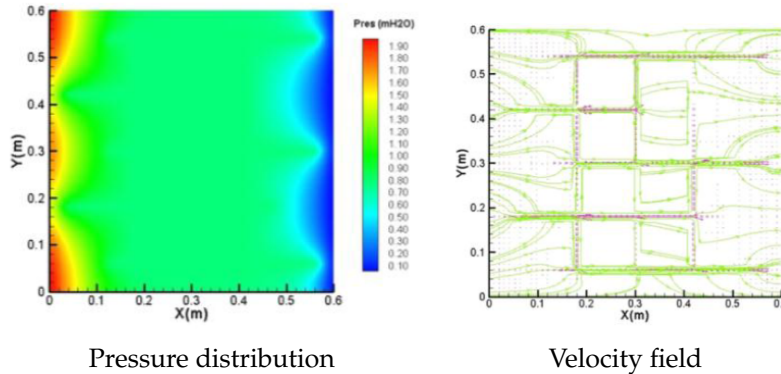
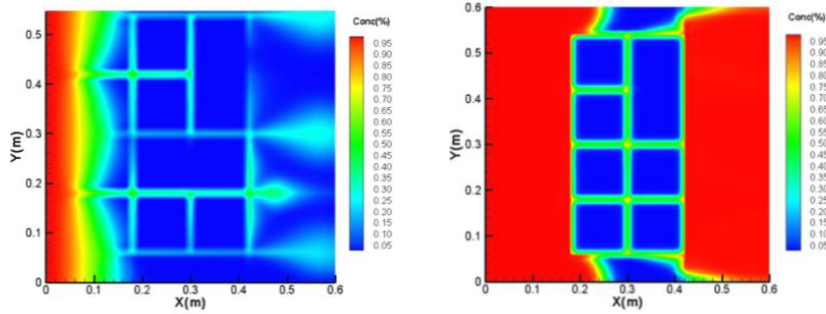


Figure 6: Pressure distribution and Velocity field for Example 4.2.



Concentration distribution at 300 year Concentration distribution at 5000 year
 Figure 7: Concentration at different time within ten thousand years.

Example 4.3. Random generated fracture network without touching boundary The model parameters employed in this base case are listed in Table 1 and we attempt to simulate up to 10,000 years. The fracture network is randomly generated but not extending to the boundary (Fig. 9) and the fracture density is 16.36081. We generate non-uniform rectangular mesh for this fractured media due to efficiency. As described before, we apply RT_0 -MFE for the flow equation, and semi-implicit FVM-MFE for the transport equation using a uniform time step of 100 years. Fig. 10 presents results of simulated concentration profiles at different times (300 years and 5000 years). At 100

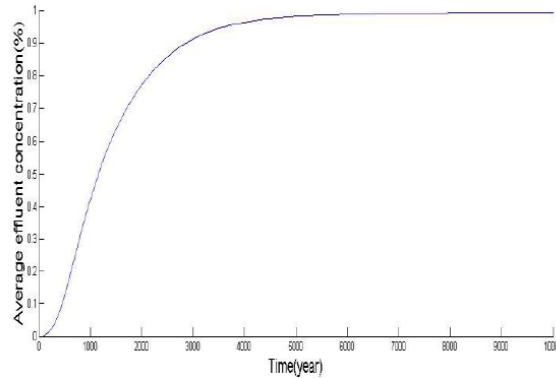


Figure 8: The flow weighted mean concentration versus time for Example 4.2.

years to 1000 years, the contaminant transports mainly through the convection within fractures. This is clearly demonstrated by the concentration plume formed quickly at the fracture outlets while the matrix closer to the inflow boundary is still quite clean. After 2,000 years, diffusion and convection via the matrix also start to play a significant role in the overall contaminant transport behavior.

The flow weighted mean concentration in effluent fluid as a function of time is provided in Fig. 11. We note that the flow weighted mean concentration quickly increases to 0.999, and then slowly approaches to 1. This is because the fracture network here

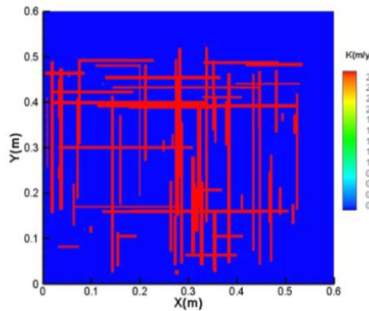
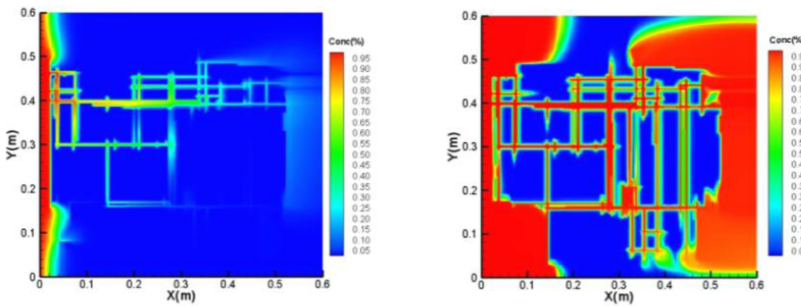


Figure 9: Fracture and conductivity distribution for Example 4.3.



Concentration distribution at 300 year Concentration distribution at 5000 year

Figure 10: Concentration at different time within ten thousand years.

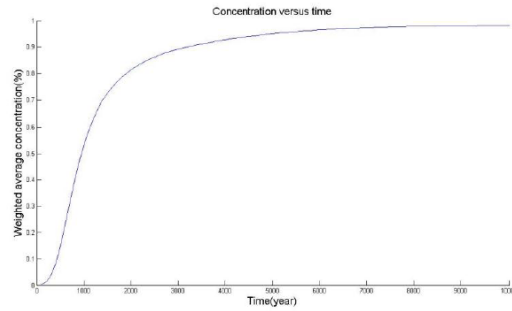


Figure 11: The flow weighted mean concentration versus time for Example 4.3.

connects inflow and outflow boundaries, which creates a flow shortcut and leads to almost all fluid exiting from the cracks rather than from the matrix.

Example 4.4. Random generated fracture network extending to boundary

In this example, we still employ the model parameters listed in Table 1 and we also simulate up to 10,000 years. We apply RT_0 -MFE on rectangular meshes for the flow equation, and semi-implicit FVM-MFE for the transport equation using a uniform time step of 100 years. The fracture network (Fig. 12) in this example is extending to the boundary and the fracture density is 24.49502. Fig. 13 shows are results of simulated concentration profiles at different times (300 years and 5000 years) from

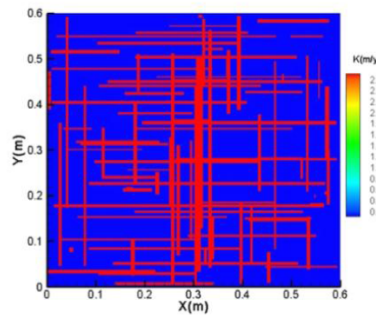
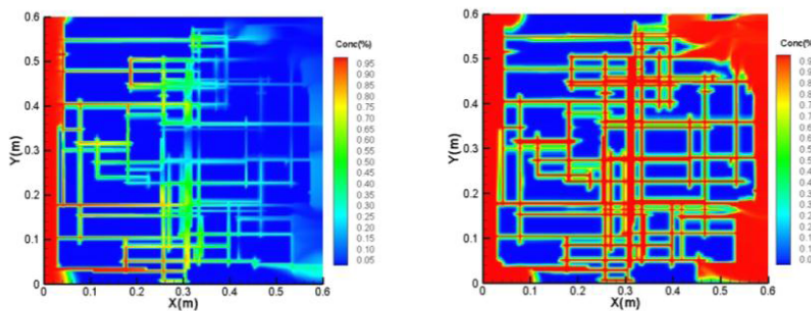


Figure 12: Fracture and conductivity distribution for Example 4.4.



Concentration distribution at 300 year Concentration distribution at 5000 year

Figure 13: Concentration at different time within ten thousand years.

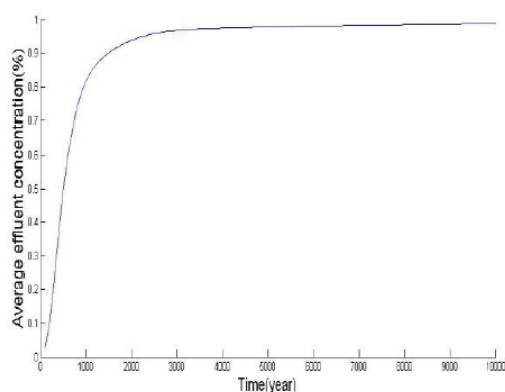


Figure 14: The flow weighted mean concentration versus time for Example 4.4.

rectangular mesh simulation. At early simulation times, the contaminant transports mainly through the convection within fractures. This is clearly demonstrated by the concentration plume formed quickly at the fracture outlets while the matrix closer to the inflow boundary is still quite clean. At later simulation times, diffusion and convection via the matrix also start to play a significant role in the overall contaminant transport behavior. Fig. 14 depicts the relationship between average effluent concentration and time. We note that the effluent concentration does not quickly increase to 0.999 within a short time, causing that our fracture network does not extend to the inflow and outflow boundaries, thus it leads our curve smoothly increasing before the contaminant species reaches the fracture network and also increasing smoothly when it comes out from fracture network, therefore we can see a breakthrough curve (a smooth step function) in this example. In about ten thousand years, the average normalized concentration on outflow boundary reaches about 99%. Through observing two graphs of average effluent concentration versus time (Fig. 11 and Fig. 14), we find that even if in the random fracture network, provided that there's one side of our fracture network touching the boundary, S-curve will increase to 99% quickly, therefore, our fracture network plays an import role in transporting contaminant species and cannot be neglected in the reality and simulation process.

4.2 Simulation examples (DG scheme)

Example 4.5. Four horizontal and two vertical fractures

We still use the same parameter as previous numerical examples and also attempt to simulate up to 10,000 years. The fracture network in this case involves four horizontal and two vertical fractures that are interconnected and does not extend to the boundary (Fig. 15). We first apply RT_0 -MFE for the flow equation, and semi-implicit FVM-MFE for the transport equation using a uniform time step of 100 years.

Fig. 16 contains results of simulated concentration profiles at different times (300 years and 5000 years). We apply RT_0 -MFE for the flow equation, and semi-implicit DG-MFE for the transport equation using a uniform time step of 100 years. Fig. 17

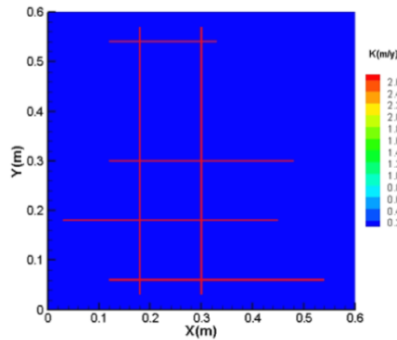
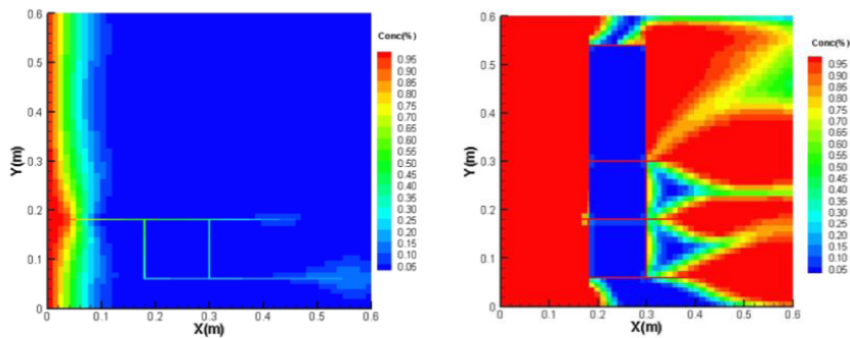


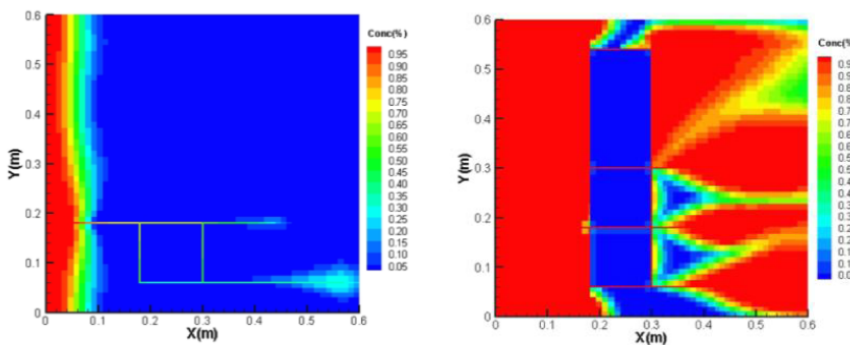
Figure 15: Fracture and conductivity distribution for Example 4.5.

shows results of simulated concentration profiles at different times under DG schemes with same simulation time. In order to demonstrate the advantage of DG scheme, we use original concentration output, which is not the post-processed data file. In Fig. 19, at simulation time 100 years, we can see that there is a gradual transition in the matrix region (outside the fracture network), but in Fig. 18, this gradual transition does not appear very obviously in the matrix region. Also, when the contaminant species



Concentration distribution at 300 year Concentration distribution at 5000 year

Figure 16: Concentration at different time within ten thousand years under MFE scheme for Example 4.5.



Concentration distribution at 300 year Concentration distribution at 5000 year

Figure 17: Concentration at different time within ten thousand years under DG scheme for Example 4.5.

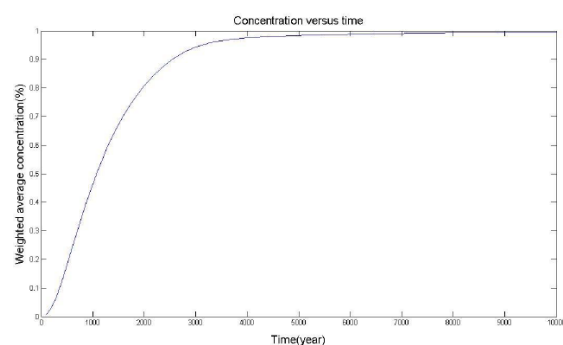


Figure 18: The flow weighted mean concentration on the outflow boundary versus time for Example 4.5 under MFE scheme.

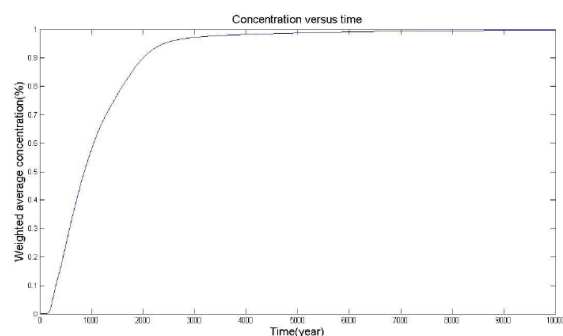


Figure 19: Same as Fig. 18 except under DG scheme.

approaches fracture network, this gradual transition will be more sharpen contrasting with picture in Fig. 18 (which is under MFE scheme). Furthermore, in the fracture network, we can still see that the gradual transition is much better than that under MFE scheme. All these facts demonstrate that DG scheme will present more detailed simulation processes than MFE scheme and therefore make our numerical results be more accurate and reliable. Figs. 18 and 19 are the pictures of the flow weighted mean concentration on the outflow boundary versus time under both MFE and DG scheme, from two pictures, we can observe that under DG scheme, S-curve will be closer to a step function which is real solution to our problem.

Example 4.6. Single fracture (without extending to the boundary)

We consider a single fracture in our domain with fracture inlet/outlet not touching the domain boundary. The fracture network is depicted in Fig. 20. We still give out the simulated concentration profiles at different times under two different schemes (Figs. 21 and 22), from those pictures (2000 years and 8000 years), we can clearly see the difference between two schemes, the simulated concentration profile under MFE scheme obviously looks more coarsely than DG scheme and covers lots of details no matter in the fracture net work or in the matrix region. In addition, we can see the picture of the average effluent concentration on the outflow boundary versus time under DG scheme will be more accurate than MFE scheme (Figs. 23 and 24), since it looks more like a step function, which is our real solution to our problem, and the

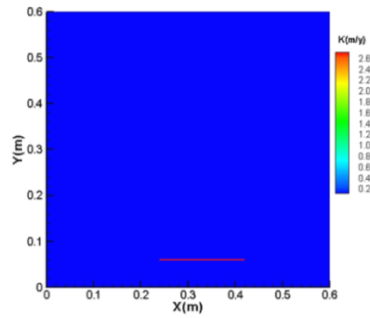
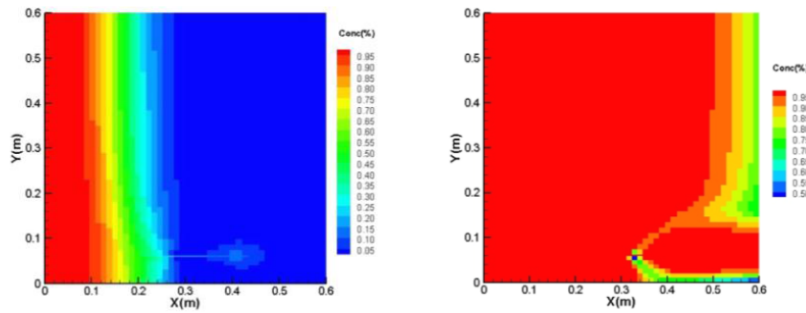
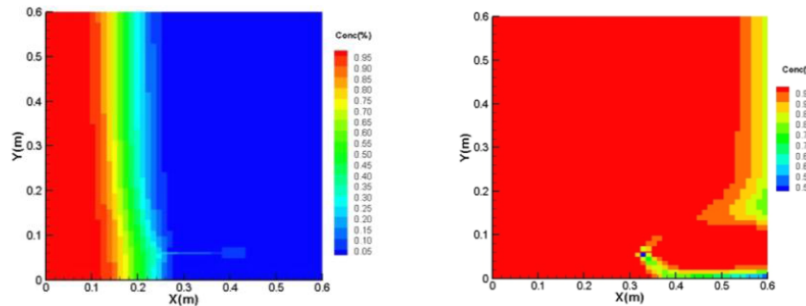


Figure 20: Fracture and conductivity distribution for Example 4.5.



Concentration distribution at 300 year Concentration distribution at 5000 year

Figure 21: Concentration at different time within ten thousand years under DG scheme for Example 4.5.



Concentration distribution at 2000 year Concentration distribution at 8000 year

Figure 22: Concentration at different time within ten thousand years under DG scheme for Example 4.5.

break through time is shorter under DG scheme than MFE scheme.

4.3 Sensitivity analysis under MFE scheme

In all sensitivity analysis, we use flow weighted mean concentration to test the influence of different parameters to our model, the flow weighted mean concentration \bar{c} is defined as follows:

$$\bar{c} = \frac{\int_{\Gamma_{outflow}} \mathbf{u} \cdot \mathbf{n} c ds}{\int_{\Gamma_{outflow}} \mathbf{u} \cdot \mathbf{n} ds}.$$

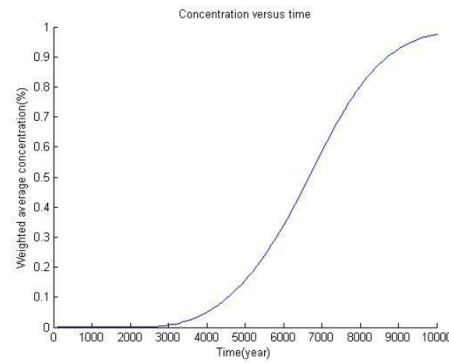


Figure 23: The flow weighted mean concentration on the outflow boundary versus time for Example 4.6 under MFE scheme.

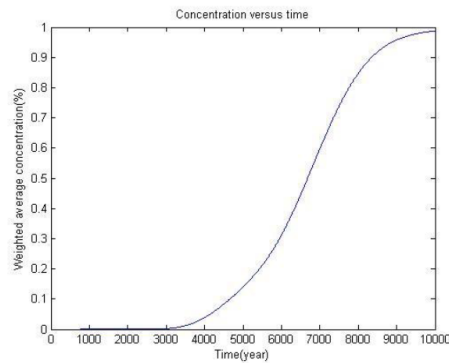


Figure 24: Same as Fig. 23 except under DG scheme.

4.3.1 Effect of K_d values

The parameter K_d value, which represents the distribution of contaminant between the solid and liquid phases, is defined as follows

$$K_d = \frac{c_s}{\bar{c}} = \frac{\text{mass of solute on the solid phase per unit mass of solid phase}}{\text{concentration of solute in solution}}.$$

The effect of the K_d expresses as a retardation in the breakthrough curve of a contaminant. Retardation of dissolved contaminant element is due to sorption, chemical reactions with porous media or fracture walls, and movement into dead-end pores by diffusion. As a result, contaminant element will not move as fast as average advective velocity of ground water which carries it. The retardation coefficient in porous media is expressed as (Freeze and Cherry, 1979; Prickett et al., 1981)

$$K_d = \frac{v}{v_c}, \quad (4.1a)$$

$$K_d = 1 + \frac{\rho_b R_d}{n}, \quad (4.1b)$$

and in fracture media (Burkholder, 1976) as

$$K_d = 1 + AR_a, \quad (4.2)$$

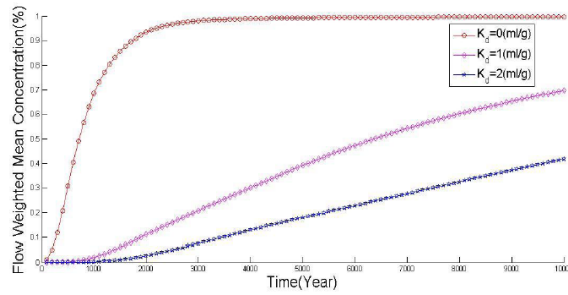


Figure 25: Sensitivity analysis for parameter K_d under MFE scheme.

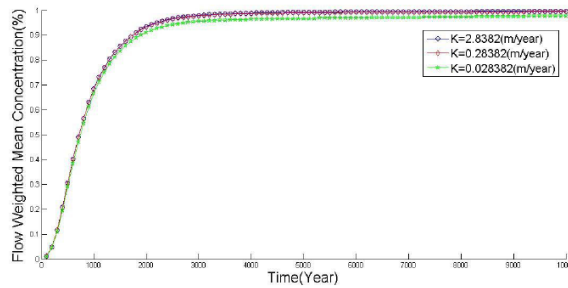


Figure 26: Sensitivity analysis for parameter conductivity under MFE scheme.

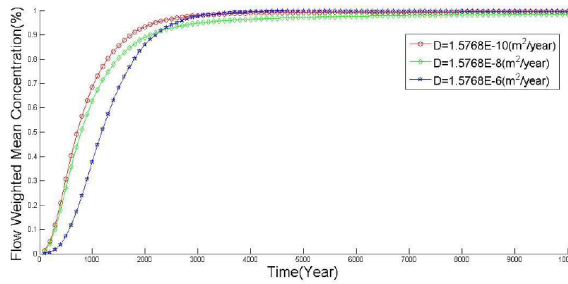


Figure 27: Sensitivity analysis for parameter diffusion coefficient under MFE scheme.

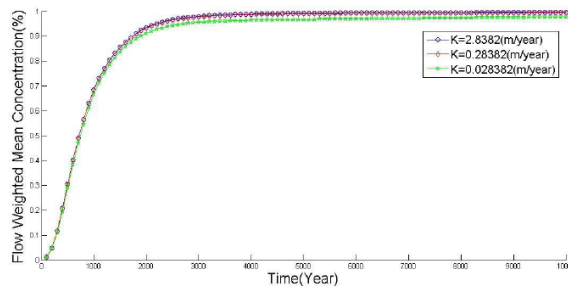


Figure 28: Sensitivity analysis for fracture density under MFE scheme.

where v = average ground-water velocity; v_c = average velocity of the contaminant mass; ρ_b = bulk mass density of the porous medium; n = effective porosity; R_d = distribution coefficient of porous medium; R_a = fracture-rock distribution coefficient; and A = ratio of fracture-wall surface area to void space (volume).

To analyze the effect of K_d values, we test three cases. Different K_d values are employed and the flow weighted mean concentrations on outflow boundary versus time are depicted in Fig. 25. Clearly, the contaminants consume less time to exit the matrix in a fractured medium with low K_d than with high K_d value.

4.3.2 Effect of conductivity

We simulate contaminant transport with three different conductivity values. The breakthrough curves for these cases are depicted in Fig. 26. From the picture we see that the exiting time of the contaminant reduces slightly in fractured medium with high conductivity values as compared to the one with lower conductivity.

4.3.3 Effect of diffusion coefficient

To analyze the effect of diffusion coefficient, we again test three cases. Different diffusion coefficient is employed and the concentrations on outflow boundary versus time are depicted in Fig. 27. Contaminant reaches the outflow boundary more quickly with a lower diffusion coefficient.

4.3.4 Effect of fracture density

We modulate various fracture density to investigate its influence. Different fracture density is employed and the concentrations on outflow boundary versus time are described in Fig. 28. Clearly and also as expected, concentration on the outflow boundary increases to 0.5 more quickly in a fractured medium with higher fracture density at in our simulation.

4.4 Lumping an entire fracture network into one equivalent crack via effective K_d

We first use our flow and contaminant transport simulator to obtain the relationship between 50% concentration time and real K_d values (Fig. 29). Here we use polynomials to fit this relationship. The resultant correlation is

$$y = 5000x + 8000,$$

where y is 50% concentration time, x is real K_d . In the second step, we get the relationship between 50% concentration time and effective K_d values (Fig. 30) for a single-fracture network:

$$y = 12500x + 1080,$$

where y is 50% concentration time, x is effective K_d . Finally, we use 50% concentration time to match relationship between effective K_d and real K_d . The final relationship we obtained is:

$$12.5u + 1.08 = 5v + 8,$$

where u denotes effective K_d , v denotes real K_d . Apparently, the relationship between the effective K_d is the real K_d is a linear relationship (also shown in Fig. 31).

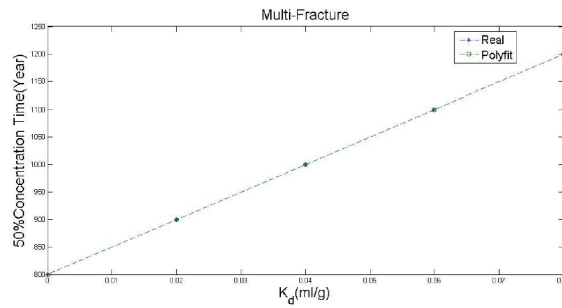


Figure 29: Relationship between 50% concentration time and real K_d .

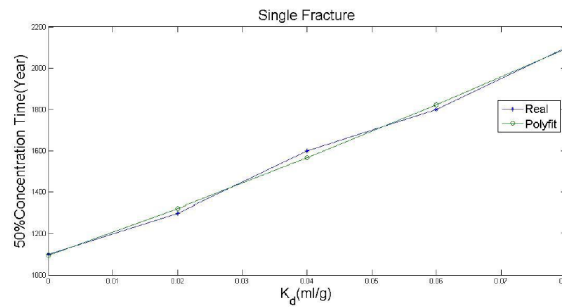


Figure 30: Relationship between 50% concentration time and effective K_d .

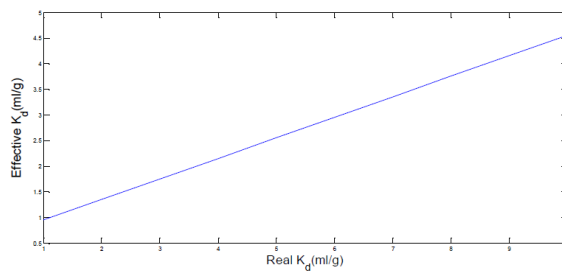


Figure 31: Effective K_d versus intrinsic K_d .

4.5 Relationship between lumped effective K_d and fracture density

In order to find this relationship between lumped effective K_d and fracture density, we first get the relationship between 50% concentration time and fracture density (Fig. 32) under multi-fracture network. Like above, we still use polynomials to fit this relationship. From Fig. 32 we can see that this relationship is kind of linear relationship, although there's some discrepancy around real curves, it can be considered as a linear relation due to the numerical errors of our simulator. The resultant correlation is

$$y = 62.7x + 1527.3,$$

where y is 50% concentration time, x is fracture density. In the second step, we get the relationship between 50% concentration time and effective K_d values (Fig. 33) for

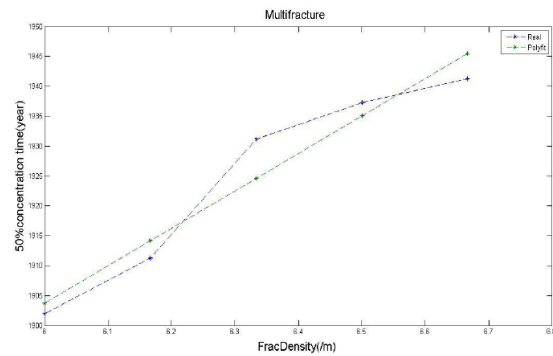


Figure 32: Relationship between 50% concentration time and fracture density.

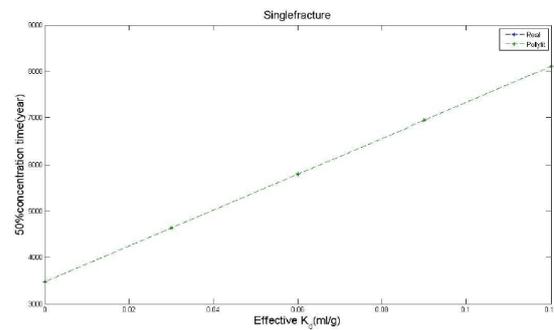


Figure 33: Relationship between 50% concentration time and effective K_d .

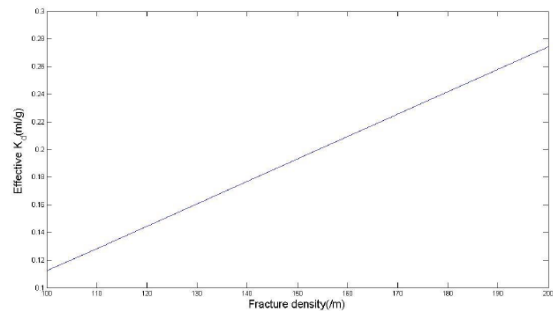


Figure 34: Effective K_d vs Fracture density.

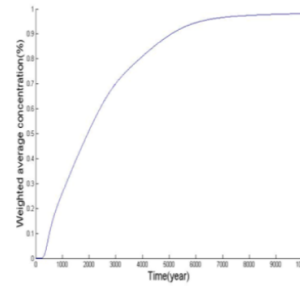
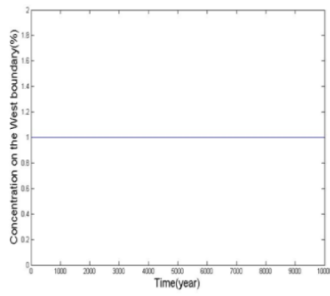
a single-fracture network:

$$y = 38588x + 3477,$$

where y is 50% concentration time, x is effective K_d . Finally, we use 50% concentration time to match relationship between effective K_d and fracture density. The final relationship we obtained is:

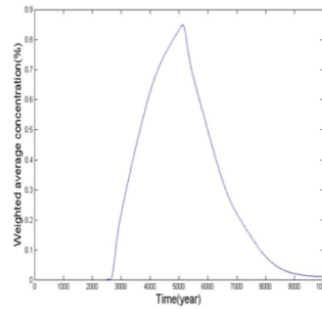
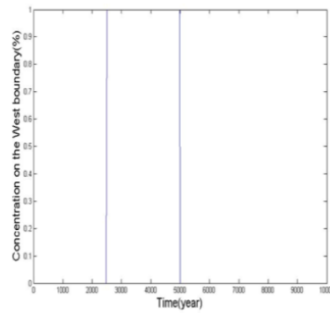
$$38.588u + 3.477 = 0.0627v + 1.5273,$$

where u denotes effective K_d , v denotes fracture density. Apparently, the relationship between the effective K_d and fracture density is a linear relationship (also shown in Fig. 34).

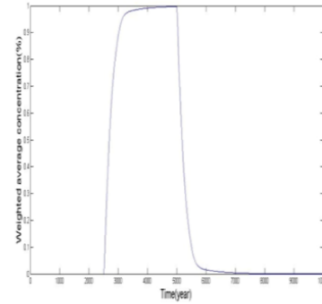
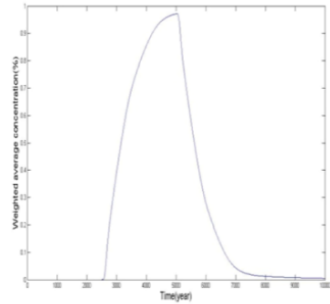


Step function of left boundary concentration Flow weighted mean concentration versus time

Figure 35: Standard case.

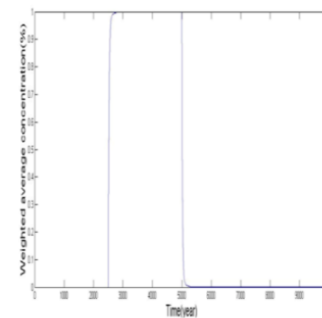
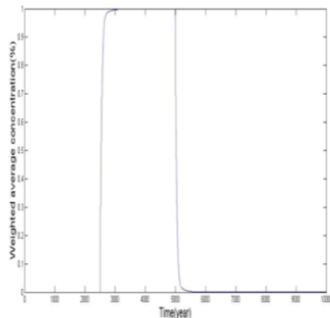


Step function of left boundary concentration Flow weighted mean concentration versus time



Left boundary pressure at 3 mH_2O

Left boundary pressure at 10 mH_2O



Left boundary pressure at 50 mH_2O

Left boundary pressure at 100 mH_2O

Figure 36: Flow weighted mean concentration versus time at different boundary pressure.

4.6 Impact of disturbed initial concentration on our model

In the previous numerical examples, we have assumed that the concentration of contaminant species is a constant on the boundary of our matrix. However, in the practical case, concentration on the boundary may be changed with time. Thus, it is interesting to investigate the case that concentration is not a constant. To see the difference between two different cases, we will again investigate the picture of flow weighted mean concentration versus time in each case. We have already known that in the former case the graph of flow weighted mean concentration versus time was a smooth S-curve, because our fracture network and different permeability between fracture and matrix made contaminant species reach the right boundary at different time. Thus, in the first case the flow weighted mean concentration on the left boundary was a constant (Fig. 35). In the second case, we disturbed concentration on the left boundary (Fig. 36), then we used our simulator to get the graph of flow weighted concentration versus time (Fig. 36). We can clearly see that this curve did not have a S-shape, it looked like the graph of normal distribution. In this graph, we can see that this curve reached its peak at 5000 years, and the peak value was about 85 percent, which was consistent with picture of constant concentration on the left boundary at 5000 years (Fig. 36). In Fig. 35, S-curve increased smoothly to 99 percent. However, In Fig. 36, we have seen that after 5000 years, the curve dropped smoothly from 85 percent into about 0 percent due to the disturbed concentration. Thus, we can see that the flow weighted mean concentration curve is related to disturbed initial concentration.

5 Conclusions and future work

In this paper, an efficient and robust simulator has been developed for the solution of contaminant species passing through a fractured cementitious matrix. We first present our mathematical model consisting of two differential equations, i.e., the flow equation and the reactive transport equation. A numerical scheme based on the MFE method is developed to approximate the second-order partial derivate terms in the flow and transport equations. The convection term in the transport equation is treated using an upwind FVM and DG method. With the MFE method, the fluxes through fractures are accurately approximated using non-uniformed rectangular mesh, because rectangular grids have the advantages of efficient vectorization for computation. Various patterns of fractures are simulated and compared. In the rectangular simulations, we employ non-uniform meshes with small elements representing cracks. Sensitivity analysis has been carried out for the analysis of each parameter's impact on our models. The effective K_d calculation for lumping an entire crack network to an equivalent single-fracture system has been proposed using our contaminant transport simulator on rectangular meshes. We also investigate the relationship between lumped effective K_d and fracture density on rectangular meshes, which we believe is meaningful and useful to our applications because the fracture network plays a crucial rule in the contaminant transport system and it tightly interacts with many other

parameters in our mathematics model such as conductivity, porosity and intrinsic K_d , thus affecting the lumped effective K_d . At last, we impose a disturbed initial concentration into our clean matrix and we see an interesting result as described in Section 4.7. In the near future, we plan to design a multi-scale scheme for efficiency.

Appendix

A Mixed finite element method

For simplicity, we consider only two dimensional rectangular domain and we only consider rectangular mesh. However, the results can be directly extended to logically rectangular domain/mesh by conforming mapping. Although we can employ different domain partitions for flow and transport problems respectively, the same non-uniform rectangular partition is considered for both flow and transport equations. The permeability tensor is assumed to be invertible and uniformly positive definite and uniformly bounded. Viscosity μ is considered to be constant in our simulation.

Before giving out the variational form of our problem, we first introduce some abstract spaces, which are used to formulate mixed finite element scheme:

$$W = L^2(\Omega) = \left\{ v : \int_{\Omega} v^2 dx < \infty \right\}, \quad V = H(\text{div}; \Omega) = \{ \mathbf{v} \in (L^2(\Omega))^d : \nabla \cdot \mathbf{v} \in L^2(\Omega) \},$$

$$V^0 = \{ \mathbf{v} \in H(\text{div}; \Omega) : \mathbf{v} \cdot \mathbf{n} = 0 \text{ on } \partial\Omega \}, \quad V_N^0 = \{ \mathbf{v} \in H(\text{div}; \Omega) : \mathbf{v} \cdot \mathbf{n} = 0 \text{ on } \Gamma_N \},$$

where

$$\nabla \cdot \mathbf{v} = \frac{\partial v_1}{\partial x_1} + \frac{\partial v_2}{\partial x_2} + \dots + \frac{\partial v_d}{\partial x_d}.$$

The norms of the two spaces $W = L^2(\Omega)$ and $V = H(\text{div}; \Omega)$ are respectively defined by

$$\|w\| \equiv \|w\|_{L^2(\Omega)} = \left(\int_{\Omega} w^2 dx \right)^{\frac{1}{2}}, \quad w \in W,$$

$$\|v\|_V \equiv \|v\|_{L^2(\Omega)} = \{ \|v\|^2 + \|\nabla \cdot \mathbf{v}\|^2 \}^{\frac{1}{2}}, \quad \mathbf{v} \in V.$$

A.1 MFE for flow equation

We first give the weak formulation of the flow equation. The mixed variational form of the flow equation is to find $\mathbf{u} \in \mathbf{V}_N^0 + E(u_B)$, $p \in W$ such that:

$$\begin{cases} (K^{-1}\mathbf{u}, v) - (\nabla \cdot \mathbf{v}, p) = - \int_{\Gamma_D} p_B \mathbf{v} \cdot \mathbf{n} ds, & \forall \mathbf{v} \in \mathbf{V}_N^0, \quad t \in (0, T], \\ (\nabla \cdot \mathbf{u}, w) = (q, w), & \forall w \in W, \quad t \in (0, T]. \end{cases}$$

Here $E(u_B)$ is the velocity extension such that its normal component agrees with u_B on Γ_N .

For simplicity, we choose to use Raviart-Thomas (RT) space (R. A. Raviart, 1977) to discretize the above weak formulation.

For a two-dimensional rectangular mesh ε_h , the r -th order RT space is defined by

$$W_h = \left\{ w \in L^2(\Omega) : w|_E \in \mathbf{Q}_{r,r}(E), E \in \varepsilon_h \right\},$$

$$V_h = \left\{ \mathbf{v} \in H(\text{div}; \Omega) : \mathbf{v}|_E \in \mathbf{Q}_{r+1,r}(E) \times \mathbf{Q}_{r,r+1}(E), E \in \varepsilon_h \right\},$$

where $\mathbf{Q}_{r,s}(E)$ is the space of polynomials of degree less than or equal to r and s , respectively, in the first and second variables restricted to the element E , clearly, $V_h \subset V$ and $W_h \subset W$. In our numerical examples below we use RT_0 space. The MFE method for flow equation is to find

$$p_h \in L^\infty((0, T], W_h) \quad \text{and} \quad \mathbf{u}_h \in L^\infty((0, T], V_{N,h}^0 + E(u_B)),$$

such that

$$\begin{cases} (K^{-1}\mathbf{u}, v) - (\nabla \cdot \mathbf{v}, p_h) = - \int_{\Gamma_D} p_B \mathbf{v} \cdot \mathbf{n} ds, & \forall \mathbf{v} \in V_{N,h}^0 \\ (\nabla \cdot \mathbf{u}_h, w) = (q, w), & \forall w \in W. \end{cases}$$

A.2 MFE and FVM for reactive transport equation

Like above, we first give the weak formulation of transport equation. The weak formulation of transport equation is to find the concentration solution $c \in W$ and the diffusive flux solution $\mathbf{v} \in V_0$ such that:

$$\begin{aligned} \left(\frac{\partial \Phi^{eff} c}{\partial t}, w \right) + (\nabla \cdot \mathbf{v}, w) + \sum_E \int_{\partial E} w \mathbf{u} c^* \cdot \mathbf{n} ds - \sum_E (c \mathbf{u}, \nabla w) &= 0, \quad \forall w \in W, \quad t \in (0, T], \\ (-D^{-1} \mathbf{v}, \hat{\mathbf{v}}) + (c, \nabla \cdot \hat{\mathbf{v}}) &= 0, \quad \forall \hat{\mathbf{v}} \in V^0, \quad t \in (0, T], \\ (c, w) &= (c_0, w), \quad \forall w \in W, \quad t = 0. \end{aligned}$$

Here c^* denotes the upwind value of the concentration on an edge. We will introduce its definition in the DG schemes.

The continuous-in-time MFE method for approximating the transport equation is to find $c_h \in L^\infty((0, T], W_h)$ and $\mathbf{v}_h \in L^\infty((0, T], V_h^0)$, such that:

$$\begin{aligned} \left(\frac{\partial \Phi^{eff} c_h}{\partial t}, w \right) + (\nabla \cdot \mathbf{v}_h, w) + \sum_E \int_{\partial E} w \mathbf{u} c_h^* \cdot \mathbf{n} ds - \sum_E (c_h^* \mathbf{u}, \nabla w) &= 0, \quad \forall w \in W_h, \quad t \in (0, T], \\ (-D^{-1} \mathbf{v}_h, \hat{\mathbf{v}}) + (c_h, \nabla \cdot \hat{\mathbf{v}}) &= 0, \quad \forall \hat{\mathbf{v}} \in V_h^0, \quad t \in (0, T], \\ (c_h, w) &= (c_0, w), \quad \forall w \in W, \quad t = 0. \end{aligned}$$

Further discretizing in time, we give the fully discretized algorithm for the transport equation. We partition the simulation time $(0, T]$ into m subintervals: $0 = t_0 < t_1 < \dots < t_{m-1} < t_m = T$. We let $\Delta t_k = t_k - t_{k-1}$, $\Delta t = \max \Delta t_k$. Assuming that there exists a constant C satisfying that $\Delta t \leq C \min \Delta t_k$, the transport equation

can be solved by semi-implicit Euler method in time and the combined FVM-MFE method in space. The fully discretized approximation is to find $c_{h,k} \in L^\infty((0, T], W_h)$ and $\mathbf{v}_{h,k} \in L^\infty((0, T], V_h^0)$, for $k = 0, 1, 2, \dots, m$ such that:

$$\begin{aligned} & \left(\frac{\partial \Phi^{eff} c_{h,k} - \Phi^{eff} c_{h,k-1}}{\Delta t}, w \right) + (\nabla \cdot \mathbf{v}_{h,k}, w) + \sum_E \int_{\partial E} w \mathbf{u} c_{h,k-1}^* \cdot \mathbf{n} ds \\ & - \sum_E (c_{h,k-1} \mathbf{u}, \nabla w) = 0, & \forall w \in W_h, \quad t \in (0, T], \\ & (-D^{-1} \mathbf{v}_{h,k}, \hat{\mathbf{v}}) + (c_{h,k} \nabla \cdot \hat{\mathbf{v}}) = 0, & \forall \hat{\mathbf{v}} \in V_h^0, \quad t \in (0, T], \\ & (c_{h,0}, w) = (c_0, w), & \forall w \in W, \quad t = 0. \end{aligned}$$

B Discontinuous Galerkin (DG) method

In order to formulate a DG scheme, let us firstly give broken Sobolev spaces which are natural spaces to work with the DG method. These spaces depend strongly on the partition of the domain. Let ε_h be a quasi-uniform family and possibly non-conforming partitions of our bounded polygonal domain Ω , which is composed of triangles or quadrilaterals in 2D, or a tetrahedron or hexahedra in 3D. We also require that these partitions are regular. This means that every element is convex. If h_E denotes the diameter of the element $E \in \varepsilon_h$ and h denotes the maximum diameter of a ball inscribed in each element $E \in \varepsilon_h$, there exists a constant $\rho > 0$ such that $h/h_E \leq \rho$ for every element $E \in \varepsilon_h$. We assume no element crosses the boundaries $\Gamma_{in}, \Gamma_{out}$ of our domain

The broken Sobolev Space for any real number s is defined as follows:

$$H^s(\varepsilon_h) = \{ \Phi \in L^2(\Omega) : \Phi|_E \in H^s(E), E \in \varepsilon_h \},$$

where H^s is known as a Sobolev space.

And the broken Sobolev norm is defined as follows:

$$\| \Phi \|_{H^s(\varepsilon_h)} = \left(\sum_{E \in \varepsilon_h} \| \Phi \|_{H^s(E)}^2 \right)^{\frac{1}{2}}.$$

In particular, we will use the broken gradient semi-norm:

$$\| \Phi \|_{H^s(\varepsilon_h)} = \left(\sum_{E \in \varepsilon_h} \| \nabla \Phi \|_{L^2(E)}^2 \right)^{\frac{1}{2}}.$$

Clearly, we have

$$H^s(\Phi) \subset H^s(\varepsilon_h) \quad \text{and} \quad H^{s+1}(\varepsilon_h) \subset H^s(\varepsilon_h).$$

Next, we will introduce the jumps and averages for DG schemes, which are key concepts in DG method. Let Γ_h be the set of all interior edges (for 2D domain) or faces (for 3D domain) for the sub-division ε_h . The sets of all edges or faces on Γ_{in} and Γ_{out} are

denoted by $\Gamma_{h,in}$ and $\Gamma_{h,out}$. On each edge or face $\gamma \in \Gamma_h$, we associate a unit normal vector n_γ . If edge or face is on the boundary of our domain, then n_γ is taken to be the unit normal outward vector to the boundary of our domain. If $\Phi \in H^1(\varepsilon_h)$, then the trace of Φ along any side of each element is well defined. But for two elements E_i and E_j which are neighbors and share one common side, there will be two traces of Φ along the edge or face $\gamma = \partial E_i \cap \partial E_j$. Then we need to give the definition of jumps and averages.

The average and the jump for $\Phi \in H^s(\varepsilon_h)$, $s > 1/2$ is defined as follows: Let $E_i, E_j \in \varepsilon_h$ and $\gamma = \partial E_i \cap \partial E_j \in \Gamma_h$ with n_γ exterior to E_i . Denote

$$\{\Phi\} = \frac{1}{2}((\Phi|_{E_i})|_\gamma + (\Phi|_{E_j})|_\gamma), \quad [\Phi] = (\Phi|_{E_i})|_\gamma - (\Phi|_{E_j})|_\gamma.$$

For the one dimensional case, we extend the definition of jump and average to sides that belong to the boundary :

$$\{\Phi\} = [\Phi] = (\Phi|_{E_j})|_\gamma,$$

for each $\gamma = \partial E_i \cap \partial \Omega$.

The discontinuous finite element space is taken to be

$$D_r(\varepsilon_h) \equiv \{\Phi \in L^2(\Omega) : \Phi|_E \in \mathbb{P}_r(E), E \in \varepsilon_h\},$$

where $\mathbb{P}_r(E)$ denotes the space of polynomials of (total) degree less than or equal to r on E .

The inner product in $(L^2(\Omega))^d$ or $L^2(\Omega)$ is indicated by (\cdot, \cdot) and the inner product in the boundary function space $L^2(\gamma)$ is indicated by $(\cdot, \cdot)_\gamma$. The norm $(L^p(\Omega))^d$ for a vector-value function is defined as

$$\|\mathbf{u}\|_{(L^p(\Omega))^d} = \|\|\mathbf{u}\|\|_{L^p(\Omega)},$$

where $|\cdot|$ is the standard vector norm defined by $|\mathbf{u}| = (\mathbf{u} \cdot \mathbf{u})^{1/2}$. For simplicity, the norms $\|\cdot\|_{L^2(\Omega)}$ and $\|\cdot\|_{(L^2(\Omega))^d}$ are also written as $\|\cdot\|_0$ for scalar-value and vector-value functions, respectively. The norm of $(L^p(\Omega))^{d \times d}$ for a matrix-value function is defined as

$$\|A\|_{(L^p(\Omega))^{d \times d}} = \|\|A\|_2\|_{L^p(\Omega)},$$

where $\|\cdot\|_2$ is the matrix 2-norm defined by $\|A\|_2 = \sup_{|u|=1} |Au|$.

B.1 DG for transport equation

B.1.1 Continuous in time formulation

For transport, we define the bilinear form $B(c, \omega; \mathbf{u})$ as

$$\begin{aligned}
 B(c, \omega; \mathbf{u}) &= \sum_{E \in \mathcal{E}_h} \int_E (D(\mathbf{u}) \nabla c - c \mathbf{u}) \cdot \nabla \omega - \int_{\Omega} c q^- \omega - \sum_{\gamma \in \Gamma_h} \int_{\gamma} \{D(\mathbf{u}) \nabla c \cdot \mathbf{n}_{\gamma}\} [\omega] \\
 &\quad - S_{transp} \sum_{\gamma \in \Gamma_h} \int_{\gamma} \{D(\mathbf{u}) \nabla c \cdot \mathbf{n}_{\gamma}\} [c] + \sum_{\gamma \in \Gamma_h} \int_{\gamma} c^* \mathbf{u} \cdot \mathbf{n}_{\gamma} [\omega] \\
 &\quad + \sum_{\gamma \in \Gamma_{h,out}} \int_{\gamma} c^* \mathbf{u} \cdot \mathbf{n}_{\gamma} \omega + J_0^{\sigma, \beta}(c, \omega),
 \end{aligned}$$

where the upwind value of concentration $c^*|_{\gamma}$ is defined as follows:

$$c^*|_{\gamma} = \begin{cases} c|_{E_i}, & \text{if } \mathbf{u} \cdot \mathbf{n} \geq 0, \\ c|_{E_j}, & \text{if } \mathbf{u} \cdot \mathbf{n} < 0, \end{cases}$$

for $\gamma = \partial E_i \cap \partial E_j$ and \mathbf{n}_{γ} is a unit normal vector pointing from E_i to E_j . Notice $\mathbf{u} \cdot \mathbf{n}_{\gamma}$ is continuous on the direction \mathbf{n}_{γ} , thus has well-defined value at the interface. $S_{transp} = -1$ for NIPG, $S_{transp} = 1$ for SIPG and $S_{transp} = 0$ for IIPG. Here q^+ is the injection source term and q^- is the extraction source term, i.e., $q^+ = \max(q, 0)$, $q^- = \min(q, 0)$. By definition, we have $q = q^+ + q^-$. (Actually in our model $q = 0$, thus we can omit the term relative to q in both bilinear and linear form). Because of the mixed boundary condition, the jump term penalizes the interior face only. $J_0^{\sigma, \beta}$ is the interior penalty term

$$J_0^{\sigma, \beta} = \sum_{\gamma \in \Gamma_h} \frac{\sigma_{\gamma}}{h_{\gamma}^{\beta}} \int_{\gamma} c[\omega],$$

where σ is a discrete positive function that takes constant value σ_{γ} on the edge or face γ and have upper and lower bound $\sigma^*, \sigma_* > 0$, h_{γ} denotes the size of γ and $\beta \geq 0$ is a real number.

The linear functional $L(\omega; \mathbf{u}, c)$ is defined as

$$L(\omega; \mathbf{u}, c) = \int_{\Omega} c \omega q^+ \omega - \sum_{\gamma \in \Gamma_{h,in}} \int_{\gamma} c_B \mathbf{u} \cdot \mathbf{n}_{\gamma} \omega.$$

The continuous in time DG scheme for approximating transport equation is as follows: we seek $\mathbf{u}_h \in L^{\infty}((0, T]; V_h^0(\varepsilon_h))$, $c_h \in L^{\infty}((0, T]; D_r(\varepsilon_h))$ satisfying,

$$\begin{aligned}
 \left(\Phi^{eff} \frac{\partial c_h}{\partial t}, \omega \right) + B(c_h, \omega; \mathbf{u}_h) &= L(\omega; \mathbf{u}_h, c_h), & \forall \omega \in D_r(\varepsilon_h), \quad \forall t \in (0, T], \\
 \left(\Phi^{eff} c_h, \omega \right) &= \left(\Phi^{eff} c_0, \omega \right), & \forall \omega \in D_r(\varepsilon_h), \quad t = 0.
 \end{aligned}$$

In implementation, we split the whole transport equation into two sub-equations, one is advection equation, and the other one is diffusion equation. We can treat two sub-equations with two different schemes, which will be more convenient for coding and

more accurate for the final solution. For instance, in our simulation, we apply DG scheme to advection problem and use MFE or Cell Centered Finite Difference (CCFD) method for the diffusion problem, which will render a better solution for the whole problem.

Next, we will give the semi-discrete formulation for the advection problem. We apply an upwind discretization. The upwind value of concentration function c^* is denoted above. The bilinear form for advection problem is denoted by $b(c, \omega; \mathbf{u})$:

$$b(c, \omega; \mathbf{u}) = - \sum_{E \in \mathcal{E}_h} \int_E c \mathbf{u} \cdot \nabla \omega + \sum_{\gamma \in \Gamma_h} \int_{\gamma} c^* \mathbf{u} \cdot \mathbf{n}_{\gamma} [\omega] + \sum_{\gamma \in \Gamma_{h,out}} \int_{\gamma} c^* \mathbf{u} \cdot \mathbf{n}_{\gamma} \omega.$$

The continuous in time DG scheme for approximating advection equation is as follows: we seek $\mathbf{u}_h \in L^\infty((0, T]; V_h^0(\varepsilon_h))$, $c_h \in L^\infty((0, T]; D_r(\varepsilon_h))$, satisfying,

$$\begin{aligned} (\Phi^{eff} \frac{\partial c_h}{\partial t}, \omega) + b(c_h, \omega; \mathbf{u}_h) &= L(\omega; \mathbf{u}_h, c_h), & \forall \omega \in D_r(\varepsilon_h), \quad \forall t \in (0, T], \\ (\Phi^{eff} c_h, \omega) &= (\Phi^{eff} c_0, \omega), & \forall \omega \in D_r(\varepsilon_h), \quad t = 0. \end{aligned}$$

For single element, the DG scheme is simplified as follows:

$$\int_{E \in \mathcal{E}_h} \frac{\partial \Phi^{eff} c_h}{\partial t} \omega dx + \int_{\partial E \in \Gamma_h} c_h^* \omega \mathbf{u} \cdot \mathbf{n}_{\gamma} ds - \int_{E \in \mathcal{E}_h} c_h \mathbf{u} \cdot \nabla \omega dx = 0, \quad \forall \omega \in D_r(\varepsilon_h), \quad \forall t \in (0, T].$$

After computing local matrix on each element, we assemble local matrix into stiff matrix then apply backward Euler method to compute solution for advection part.

C Cell centered finite difference method (CCFD)

We firstly solve the flow equation with cell centered finite difference method, then plug our solved velocity into reactive transport equation using FVM and CCFD deal with advection and diffusion part respectively. As we all known that "Finite volume" refers to the small volume surrounding each node point on a mesh. In the finite volume method, volume integrals in a partial differential equation that contain a divergence term are converted to surface integrals, using the divergence theorem. These terms are then evaluated as fluxes at the surfaces of each finite volume. Because the flux entering a given volume is identical to that leaving the adjacent volume, these methods are conservative. Another advantage of the finite volume method is that it is easily formulated to allow for unstructured meshes. The method is used in many computational fluid dynamics packages.

We denote $\delta_x \times \delta_y$ as a possibly non-uniform rectangular mesh

$$\delta_x : 0 = x_0 < x_1 < \dots < x_M = L_x, \quad \delta_y : 0 = y_0 < y_1 < \dots < y_M = L_y.$$

We partition the simulation time $[0, T]$ into K subintervals: $0 = t_0 < t_1 < \dots < t_{K-1} < t_K = T$. We first define center point of each subintervals:

$$x_{i+\frac{1}{2}} = \frac{1}{2}(x_i + x_{i+1}), \quad i = 0, 1, \dots, M - 1;$$

$$y_{j+\frac{1}{2}} = \frac{1}{2}(y_j + y_{j+1}), \quad j = 0, 1, \dots, N - 1.$$

We simply denote the approximate solution of $c(x_{i+1/2}, y_{j+1/2}, t_k)$ as

$$c_{i+\frac{1}{2}, j+\frac{1}{2}}^k \quad \text{for } i = 1, \dots, M - 2 \text{ and } j = 1, \dots, N - 2,$$

for the convenience to discretize flow and transport equations respectively.

With these notations, the CCFD scheme for our problem is defined as follows: For flow problem, we have following discretezied cell-centered finite difference scheme:

$$-\left[\frac{1}{x_{i+1} - x_i} \left(K_{xx} \frac{P_{i+\frac{3}{2}, j+\frac{1}{2}} - P_{i+\frac{1}{2}, j+\frac{1}{2}}}{x_{i+\frac{3}{2}} - x_{i+\frac{1}{2}}} - K_{xx} \frac{P_{i+\frac{1}{2}, j+\frac{1}{2}} - P_{i-\frac{1}{2}, j+\frac{1}{2}}}{x_{i+\frac{1}{2}} - x_{i-\frac{1}{2}}} \right) \right. \\ \left. + \frac{1}{y_{j+1} - y_j} \left(K_{yy} \frac{P_{i+\frac{1}{2}, j+\frac{3}{2}} - P_{i+\frac{1}{2}, j+\frac{1}{2}}}{y_{j+\frac{3}{2}} - y_{j+\frac{1}{2}}} - K_{yy} \frac{P_{i+\frac{1}{2}, j+\frac{1}{2}} - P_{i+\frac{1}{2}, j-\frac{1}{2}}}{y_{j+\frac{1}{2}} - y_{j-\frac{1}{2}}} \right) \right] = q.$$

For transport part, the discretezied cell-centered finite difference scheme is formulated as follows:

$$\frac{\Phi_{i+\frac{1}{2}, j+\frac{1}{2}}^{k+1} c_{i+\frac{1}{2}, j+\frac{1}{2}}^{k+1} - \Phi_{i+\frac{1}{2}, j+\frac{1}{2}}^k c_{i+\frac{1}{2}, j+\frac{1}{2}}^k}{t^{k+1} - t^k} + \left(\frac{\mathbf{u}_x c_{i+1, j+\frac{1}{2}}^{k+1} - \mathbf{u}_x c_{i, j+\frac{1}{2}}^{k+1}}{x_{i+1} - x_i} + \frac{\mathbf{u}_y c_{i+\frac{1}{2}, j+1}^{k+1} - \mathbf{u}_y c_{i+\frac{1}{2}, j}^{k+1}}{y_{j+1} - y_j} \right) \\ - \left[\frac{1}{x_{i+1} - x_i} \left(D_{xx} \frac{c_{i+\frac{3}{2}, j+\frac{1}{2}}^{k+1} - c_{i+\frac{1}{2}, j+\frac{1}{2}}^{k+1}}{x_{i+\frac{3}{2}} - x_{i+\frac{1}{2}}} - D_{xx} \frac{c_{i+\frac{1}{2}, j+\frac{1}{2}}^{k+1} - c_{i-\frac{1}{2}, j+\frac{1}{2}}^{k+1}}{x_{i+\frac{1}{2}} - x_{i-\frac{1}{2}}} \right) \right. \\ \left. + \frac{1}{y_{j+1} - y_j} \left(D_{yy} \frac{c_{i+\frac{1}{2}, j+\frac{3}{2}}^{k+1} - c_{i+\frac{1}{2}, j+\frac{1}{2}}^{k+1}}{y_{j+\frac{3}{2}} - y_{j+\frac{1}{2}}} - D_{yy} \frac{c_{i+\frac{1}{2}, j+\frac{1}{2}}^{k+1} - c_{i+\frac{1}{2}, j-\frac{1}{2}}^{k+1}}{y_{i+\frac{1}{2}} - y_{j-\frac{1}{2}}} \right) \right] = q c_{i+\frac{1}{2}, j+\frac{1}{2}}^{k+1},$$

where K_{xx}, K_{yy} are the xx -component and yy -component of permeability tensor at cell centers respectively; D_{xx}, D_{yy} are the xx -component and yy -component of diffusion coefficient tensor at cell centers respectively; $\mathbf{u}_x, \mathbf{u}_y$ are the computed x -direction and y -direction Darcy velocity (flux) respectively from flow equation; q is a constant. For general case, q in the transport part does not equal to 0, but in our simulation, we simplify it as 0 in transport because of our models. Proper discretization for boundary conditions is needed for the final formulation matrix for both flow and transport equations and finish implementation.

References

- [1] V. AIZINGER, C. N. DAWSON, B. COCKBURN AND P. CASTILLO, *The local discontinuous Galerkin method for contaminant transport*, Adv. Water. Res., 24 (2001), pp. 73–87.

- [2] T. ARBOGAST, S. BRAYANT, C. N. DAWSON, F. SAAF AND C. WANG, *Computational methods for multiphase flow and reactive transport problems arising in subsurface contaminant remediation*, J. Comput. Appl. Math., 74 (1996), pp. 19–32.
- [3] T. ARBOGAST AND M. F. WHEELER, *A characteristics-mixed finite element method for advection dominated transport problems*, SIAM J. Numer. Anal., 32 (1995), pp. 404–424.
- [4] T. ARBOGAST, M. F. WHEELER AND N. Y. ZHANG, *A nonlinear mixed finite element method for a degenerate parabolic equation arising in flow in porous media*, SIAM J. Numer. Anal., 33 (1996), pp. 1669–1687.
- [5] A. K. AZIZ AND J. L. LIU, *A Galerkin method for the forward-backward heat equation*, Math. Comput., 56 (1991), pp. 35–44.
- [6] A. K. AZIZ AND P. MONK, *Continuous finite element in space and time for the heat equation*, Math. Comput., 52 (1989), pp. 255–274.
- [7] L. C. COWSAR, T. F. DUPONT AND M. F. WHEELER, *A priori estimates for mixed finite element methods for the wave equation*, Comput. Methods. Appl. Mech. Eng., 82 (1990), pp. 205–222.
- [8] Z. CHEN, *Finite Element Methods and Their Applications*, Springer-Verlag, Heidelberg, ISBN-3-540-24078-0.
- [9] C. N. DAWSON, *Godunov-mixed methods for advection-diffusion equations in one space dimension*, SIAM J. Numer. Anal., 28 (1991), pp. 1282–1309.
- [10] C. N. DAWSON, *Analysis of an upwind-mixed finite element method for nonlinear contaminant transport equations*, SIAM J. Numer. Anal., 35(5) (1998), pp. 1709–1724.
- [11] C. N. DAWSON, S. SUN AND M. F. WHEELER, *Compatible algorithms for coupled flow and transport*, Comput. Methods. Appl. Mech. Eng., 193 (2004), pp. 2565–2580.
- [12] C. DONG, S. SUN AND G. A. TAYLOR, *Numerical modeling of contaminant transport in fractured porous media using mixed finite element and finite volume methods*, J. Porous. Media., 14(3) (2011), pp. 219–242.
- [13] J. O. DUGUID AND P. C. Y. LEE, *Flow in fractured porous media*, Water. Res. Research., 13(3) (1977), PP. 558–566, doi:10.1029/WR013i003p00558.
- [14] D. A. FRENCH AND T. E. PETERSON, *A continuous space-time finite element method for the wave equation*, Math. Comput., 65 (1996), pp. 491–506.
- [15] C. GALLO AND G. MANZINI, *2D Numerical modeling of bioremediation in heterogeneous saturated soils*, Trans. Porous. Media., 31 (1998), pp. 67–88.
- [16] C. GALLO AND G. MANZINI, *Mixed finite element/volume approach for solving biodegradation transport in groundwater*, Int. J. Number. Meth. Fluids., 26 (1998), pp. 533–556.
- [17] R. GLOWINSKI, W. A. KINTON AND M. F. WHEELER, *A mixed finite element formulation for boundary controllability of the wave equation*, Int. J. Numer. Methods. Eng., 27 (1989), pp. 623–635.
- [18] L. JIANG AND I. D. MISHEV, *Mixed multiscale finite volume methods for elliptic problems in two-phase flow simulations*, Commun. Comput. Phys., 11 (2012), pp. 19–47.
- [19] Q.-J. KANG, P. C. LICHTNER AND D. R. JANECKY, *Lattice Boltzmann Method for Reacting Flows in Porous Media*, Adv. Appl. Math. Mech., 2 (2010), pp. 545–563.
- [20] J. KIM AND M. DEO, *Finite element, discrete fracture model for multiphase flow in porous media*, AIChE J., 46(6) (2000), pp. 1120–1130.
- [21] M. KARIMIFARD AND A. FIROOZABADI, *Numerical simulation of water injection in 2-d fractured media using discrete-fracture model*, SPE Reservoir. Eval. Eng., 4 (2003), pp. 117–126.
- [22] W. J. LAYTON, F. SCHIEWECK AND I. YOTOV, *Coupling fluid flow with porous media flow*, SIAM J. Numer. Anal., 40(6) (2003), pp. 2195–2218.
- [23] S. NAKAYAMA, I. TAKAGI AND K. HIGASHI, *A semi-analytical solution for advection-*

- dispersion migration of radionuclides through two-layered geologic media*, Mere. Fac. Eng., 48 (1986), pp. 227–239.
- [24] M. SAHIMI, *Flow and Transport in Porous Media and Fractured Rock: From Classical Methods to Modern Approaches*, 1995.
- [25] P. SIEGEL, R. MOSE, P. ACKERER AND J. JAFFRE, *Solution of the advection-diffusion equation using a combination of discontinuous and mixed finite element*, Int. J. Numer. Meth. Fluids., 24 (1997), pp. 595–613.
- [26] S. SUN, *Discontinuous Galerkin Methods for Reactive Transport in Porous Media*, Ph.D. dissertation, The University of Texas at Austin, 2003.
- [27] S. SUN, B. RIVIERE AND M. F. WHEELER, *A combined mixed finite element and discontinuous Galerkin method for miscible displacement problems in porous media*, in: Proceedings of International Symposium on Computational and Applied PDEs held at Zhangjiajie National Park of China, pp. 321–348, 2002.
- [28] S. SUN AND M. F. WHEELER, *Discontinuous Galerkin methods for coupled flow and reactive transport problems*, Appl. Numer. Math., 52(2-3) (2005), pp. 273–298.
- [29] S. SUN AND M. F. WHEELER, *A posteriori error estimation and dynamic adaptivity for symmetric discontinuous Galerkin approximations of reactive transport problems*, Comput. Methods. Appl. Mech. Eng., 195 (2006), pp. 632–652.
- [30] S. SUN AND M. F. WHEELER, *Projections of velocity data for the compatibility with transport*, Comput. Methods. Appl. Mech. Eng., 195 (2006), pp. 653–673.
- [31] S. SUN AND M. F. WHEELER, *A dynamic, adaptive, locally conservative and nonconforming solution strategy for transport phenomena in chemical engineering*, Chem. Eng. Commun., 193(12) (2006), pp. 1527–1545.
- [32] S. SARKAR AND M. N. TOKSÖZ, *Fluid Flow Simulation in Fractured Reservoirs*, Report, Annual Consortium Meeting, 2002.
- [33] M. YU AND D. E. DOUGHERTY, *FCT Model of contaminant Transport on Unstructured Meshes*, Volume 1, pp. 199–206, Computational Mechanics Publications, 1998.